

# Journal Pre-proof

End-to-end design of a robust attitude control and vibration suppression system for large space smart structures

Federica Angeletti, Paolo Iannelli, Paolo Gasbarri, Marco Sabatini



PII: S0094-5765(21)00152-1

DOI: <https://doi.org/10.1016/j.actaastro.2021.04.007>

Reference: AA 8606

To appear in: *Acta Astronautica*

Received Date: 7 January 2021

Revised Date: 14 March 2021

Accepted Date: 6 April 2021

Please cite this article as: F. Angeletti, P. Iannelli, P. Gasbarri, M. Sabatini, End-to-end design of a robust attitude control and vibration suppression system for large space smart structures, *Acta Astronautica* (2021), doi: <https://doi.org/10.1016/j.actaastro.2021.04.007>.

This is a PDF file of an article that has undergone enhancements after acceptance, such as the addition of a cover page and metadata, and formatting for readability, but it is not yet the definitive version of record. This version will undergo additional copyediting, typesetting and review before it is published in its final form, but we are providing this version to give early visibility of the article. Please note that, during the production process, errors may be discovered which could affect the content, and all legal disclaimers that apply to the journal pertain.

© 2021 Published by Elsevier Ltd on behalf of IAA.

## End-to-end design of a robust attitude control and vibration suppression system for large space smart structures

Federica Angeletti<sup>a\*</sup>, Paolo Iannelli<sup>a</sup>, Paolo Gasbarri<sup>b</sup>, Marco Sabatini<sup>c</sup>

<sup>a</sup> *Department of Mechanical and Aerospace Engineering (DIMA), Sapienza University of Rome, via Eudossiana 18, 00184, Rome, Italy*

[federica.angeletti@uniroma1.it](mailto:federica.angeletti@uniroma1.it)<sup>\*</sup>, [paolo.iannelli@uniroma1.it](mailto:paolo.iannelli@uniroma1.it)

<sup>b</sup> *School of Aerospace Engineering, Sapienza University of Rome, Via Salaria 851, 00138, Rome, Italy*

[paolo.gasbarri@uniroma1.it](mailto:paolo.gasbarri@uniroma1.it), [marco.sabatini@uniroma1.it](mailto:marco.sabatini@uniroma1.it)

<sup>c</sup> *Department of Astronautics Engineering, Electrical and Energy (DIAEE), Sapienza University of Rome, via Eudossiana 18, 00184, Rome, Italy*

\* Corresponding Author

### Abstract

The standard approach of controlling in-orbit large flexible structures only by adopting actuators and sensors located at platform level is currently being challenged by new missions' stringent requirements in terms of demanding guidance profiles and instrument performance. In this perspective, smart materials offer a different solution to improve the performance of space systems by controlling the vibrations of such lightweight structures. In this paper, the problem of designing an end-to-end architecture for active control of large in-orbit structures is addressed. First, a FE model of a large space antenna is derived by using commercial software. The instrument is designed to be supported by an active deployable frame hosting an optimal minimum set of collocated smart actuators and sensors. To this purpose, a comparison among different placement techniques, as Gramian and Modal Strain Energy (MSE) based methods, is proposed to find the final configuration for both actuators and sensors. Attention is paid to create a GNC strategy combining collocated control on flexible appendages with platform control, while minimizing the relative displacements among the most critical points of the antenna. To achieve high performance, Linear Fractional Transformation (LFT) modelling and advanced multivariable techniques are implemented. Finally, to validate the proposed controller, the control system is tested by simulating typical spacecraft manoeuvre profiles.

### 1. Introduction

Nowadays, the standard approach of controlling large space flexible structures only by implementing actuators and sensors at platform level is being more and more challenged by new missions narrow constraints in terms of pointing, guidance and calibration profiles. Indeed, modern spacecraft are required to perform high resolution geospatial services without incurring in geometric distortions or communication issues related to undesired elastic vibrations. In parallel, most of Earth observation (EO) missions are being equipped with increasingly extended flexible scientific instruments and antenna structures, whose flexibility provokes issues related to Control/Structure interactions [1][2]. In such cases, spacecraft flexible modes are very low and coupled around all control axis of the spacecraft, thus demanding a new active control strategy to increase their damping and to guarantee performance requirements are fulfilled. Indeed, according to the current state of the art for space missions with very low frequencies, controllers with low control bandwidths, limit on the input force and torque commands or passive devices are used to minimize the impact of flexible modes on spacecraft dynamics [3].

A different school of thoughts looks for actively stiffening the structure by implementing smart vibration

control devices, thus avoiding the need, time and costs for a structure-control iterative design process and for implementing stiffer and more massive structures [10]. However, currently, most of the wide space structures are sustained by passive materials, without putting into effect intelligent systems able to counteract external disturbances generated by the motion of the rigid base of the spacecraft and by environmental disturbances, as solar radiation pressure, gravity gradient torques and thermal gradients. In this context, research has been carried out to validate such an approach, by recurring to three distinct methods: independent attitude controllers, minimizing disturbance originated by the flexible parts (such as classical PID feedback with filters [4], Robust controllers [5]), vibration controllers, working in parallel to platform actuators (Direct Velocity Feedback methods [7], Positive Position Feedback [8], Pole/Zero Assignment [9], Machine Learning-based [10] among others) and combined controllers (as Synergetic methods [11] and wave-based controllers [6]), less often seen in literature.

In this paper, a control-oriented strategy to design a in parallel attitude and active vibration control (AVC) system suitable to spacecraft equipped with generically-shaped flexible appendages is proposed. In detail, this research aims at contributing to the current state of the art by suggesting a general and straightforward end-to-end design methodology. The first step is the design of a

flexible antenna, followed by an optimal placement procedure for collocated smart actuators/sensors, suitable to a wide variety of current flexible payloads. Then, control synthesis and validation steps are carried out, proposing and testing on a non-linear model a Robust controller tailored for attitude control needs, working simultaneously to a vibration suppression controller. Furthermore, as opposed to most of available literature addressing vibration suppression and attitude control for satellites, which generally refers to simple geometric shapes as beams and plates, this work selected as representative study case a 3-D mesh antenna. Such a structure is characterized by a circular truss supporting a large parabolic reflector, usually with diameter higher than 6 meters (as the AstroMesh® family). Indeed, a growing interest is currently being addressed at European level towards such a type of structure, as proved by the development of a LEA (Large European Antenna) project in the frame of a Horizon 2020 project.

The paper is organised as follows: in Section 2 a Large Mesh Reflector Model (LMRM) is designed and selected to test the proposed strategy. In Section 3, both non-linear and linearized spacecraft dynamics are presented. In Section 4, the general procedure for the placement of collocated actuators/sensors for a flexible 3-D structure is described. In Section 5, the combined control of the spacecraft is illustrated, while Section 6 reports the main results of an attitude manoeuvres with active vibration suppression. Finally, the conclusions are drawn in Section 7.

## 2. Large Mesh Reflector Model (LMRM)

A realistic representative model of the dynamic behaviour of a mesh reflector is developed as a study case to test the control strategy proposed in this paper. Indeed, based on available information [12][13], a Replica Model (RM) of the 12-meters diameter AstroMesh® reflector is realized in a finite element simulation environment (namely MSC Nastran). The comparison between the main dynamic features of the two systems is reported in Table 1. In detail, the antenna is supported by a truss structure composed of 30 unit bays. The reflector parabolic surface (with an areal density of about 0.3 kg/m<sup>2</sup>) is thought to be sustained by a net of rod elements representing AstroMesh® actual cable mesh. The truss horizontal and vertical tubes are assumed to be 2.5 meters long, while the diagonal ones 2.81 meters. The material of the truss is Carbon Fiber Reinforced Polymer (CFRP), with density equal to 1650 kg/m<sup>3</sup> and Young modulus 125 GPa. The cable mesh rod elements, in CFRP material, have an area equal to 1 mm<sup>2</sup>.

To exploit the advantages an active control solution may induce on the system design, a lighter reflector model, namely LMRM, was derived based on the RM.

Indeed, the objective was to guarantee a relevant mass reduction (established as the 30% of the initial mass), while still maintaining the same modal shapes and stiffness distribution identified in the Replica Model (see Fig. 1 and Table 2). Indeed, the truss tubes external radius  $r_{ext}$  and internal radius  $r_{int}$  have been reduced by 1 cm and material density has been slightly decreased, yet maintaining the same material type (CFRP). The characteristics of the RM and LMRM are listed in Table 2.

Table 1. Comparison between different models

	AstroMesh® data	Replica Model	LMRM
Mass (kg)	Truss: 53	Truss: 53.01	Truss: 38.34
	Mesh: 4.1	Mesh: 4.25	Mesh: 4.25
	Total: 57.1	Total: 57.26	Total: 42.6
1 <sup>st</sup> Mode (Hz)	Truss: 0.30	Truss: 0.30	Truss: 0.20
	Truss+Mesh: 0.80	Truss+Mesh: 0.78	Truss+Mesh: 0.53

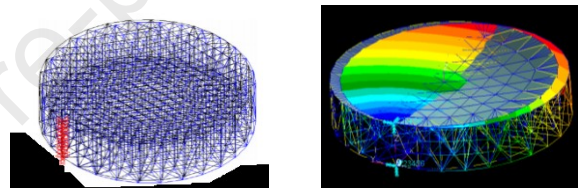


Fig. 1. (Left) First mode of the antenna truss [13]; (Right) First mode of the LMRM

Table 2. Geometry and material characteristics

	Replica Model		LMRM	
	$r_{ext}$	$r_{int}$	$r_{ext}$	$r_{int}$
Horizontal/Vertical tubes radius (mm)	31	30	21	20
Diagonal tubes radius (mm)	21	20	10	9
Density (kg/m <sup>3</sup> )	1650		1550	
Young modulus (GPa)	125		125	

To ensure a correct deployment of the reflector and to support the antenna when in-orbit, an extendable boom is generally implemented on the spacecraft platform. Therefore, an 8-meter long, 20 kg boom has been included in the structural model of the LMRM, which has been chosen as study case. As specified in [12], the deployed payload, composed of boom and the reflector, has generally three distinct constrained mode, named yaw, pitch and roll modes. They correspond to torsion and bending with respect to the main coordinated axes, illustrated in Fig. 2 along with a complete model of the payload. Usually, the yaw is the first fundamental mode, and it is often close to the pitch

mode, while the roll one is larger than the others. Concerning the available data in [12], the order of the modes for the clamped system is: yaw, pitch and roll, while the related frequencies are not available. Nevertheless, having compared the behaviour of the mesh reflector with the original AstroMesh® model, it is reasonable to assume the dynamics behaviour are similar. Indeed, the same order of natural modes can be found in Table 3 when referring to the study case and its modal shapes.

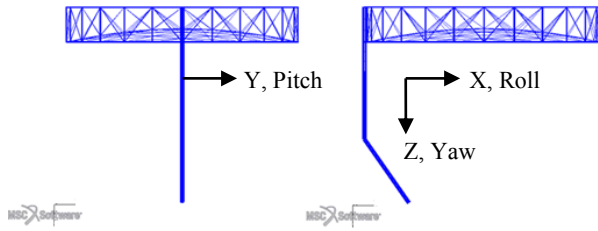
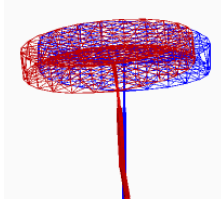
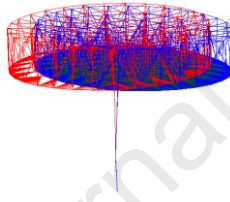
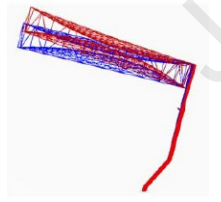
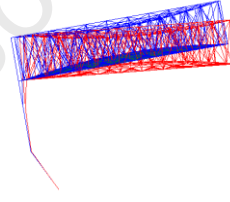
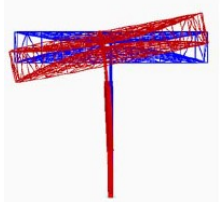
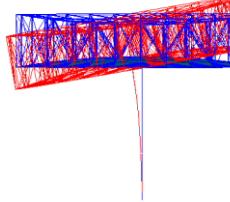


Fig. 2. Lateral views of the LMRM

Table 2. Clamped modes and frequencies

Mode	AstroMesh®	LMRM replica
1 <sup>st</sup>	 <p>Yaw mode: bending about Z axis [1] Frequency: n.a.</p>	 <p>Yaw mode: bending about Z axis Frequency: 0.41 Hz</p>
2 <sup>nd</sup>	 <p>Pitch mode: bending about Y axis [1] Frequency: n.a.</p>	 <p>Pitch mode: bending about Y axis Frequency: 0.53 Hz</p>
3 <sup>rd</sup>	 <p>Roll mode: torsion about X axis [1] Frequency: n.a.</p>	 <p>Roll mode: torsion about X axis Frequency: 0.85 Hz</p>

In the next sections, the equations of motion for a spacecraft equipped with a flexible appendage will be

presented, thus allowing us to introduce the problem of the optimal placement of collocated actuators/sensor on a generic flexible tri-dimensional structure. This approach will be further tested on the proposed LMRM.

### 3. Dynamics of the Assembled Spacecraft

It is possible to derive nonlinear dynamic equations of straightforward use for flexible spacecraft attitude control problems by adopting a Lagrangian approach [14][15]. For brevity's sake, only the final equations of motion are reported in this paper, as the steps leading to such formulation may already be found in [16][17][18]. In general, a state vector is identified as  $X = [X_G, \Theta, \eta]$ , where  $X_G$  indicates the position of the platform center of gravity G with respect to an ECI inertial frame,  $\Theta$  the attitude of the body reference frame with respect to the inertial system and  $\eta$  the modal amplitudes of a flexible appendage equipped to a central satellite platform.

Therefore, the full non-linear dynamics of the system can be written as reported in eq. (1).

$$M_T^G \ddot{C}_i + N_{L,T} = F_T^G \quad (1)$$

In detail, the system total mass matrix reads as

$$M_T^G = \begin{bmatrix} (m_{A_i} + m_b) \mathbf{I} & {}^B \tilde{\mathbf{p}}_{i,c} & \mathbf{L}_k^A \\ ({}^B \tilde{\mathbf{p}}_{i,c})^T & {}^B \tilde{\mathbf{J}}_{G,i,O_i} & \tilde{\mathbf{S}}_k \\ {}^B \mathbf{L}_k^{A,T} & {}^B \tilde{\mathbf{S}}_k & \mathbf{I} \end{bmatrix} \quad (2)$$

with  $m_b$  mass of the platform,  $m_{A_i}$  mass of the appendage,  ${}^B \tilde{\mathbf{p}}_{i,c}$  static moment of the system with respect to the platform center of gravity G, defined in the body reference frame,  ${}^B \tilde{\mathbf{J}}_{G,i,O_i}$  moment of inertia of the system with respect to G in the body frame,  ${}^B \mathbf{L}_k^A$  and  ${}^B \tilde{\mathbf{S}}_k$  translation and rotation modal participation factors (coupling with the rigid motion),  $\mathbf{I}$  is the identity matrix.

Furthermore, the matrices  $\mathbf{C}_T$  and  $\mathbf{K}_T$  are defined as

$$\mathbf{C}_T = \begin{bmatrix} 0 & 0 & 0 \\ 0 & 0 & 0 \\ 0 & 0 & 2\Sigma\Omega \end{bmatrix}, \quad \mathbf{K}_T = \begin{bmatrix} 0 & 0 & 0 \\ 0 & 0 & 0 \\ 0 & 0 & \Omega^2 \end{bmatrix} \quad (3)$$

where  $\Omega$  is a diagonal matrix listing all squared angular frequencies of the appendages as cantilevered to satellite and  $\Sigma$  is a diagonal matrix containing the  $k$ -th damping factor  $\xi_k$  of the corresponding elastic mode.

The term  $F_T^G$  indicates the generalized forces (forces  $f_G$ , torques  $c_G$  and projection of forces on the modal base  $\tilde{\mathbf{S}}_k$ ) applied to the spacecraft in G. In case of a flexible structure equipped with smart actuators, the forces exerted by the active devices on the modal base, originated by multiplying the electro-mechanical

coupling matrix  $\tilde{\mathbf{K}}_{U\psi}$  (see Par. 3.2) and the input voltage  $\psi$  vector, are included in the following expression

$$F_T^G = [f_G, c_G, \tilde{\psi} \cdot \tilde{\mathbf{K}}_{U\psi}^T]^T \quad (4)$$

Finally, the non-linear terms are indicated below as

$${}^B N_L^G = \begin{bmatrix} \omega \wedge (\omega \wedge \tilde{I}_T^G) + \sum_{k=1}^N {}^B L_k^A \dot{\theta}_k \\ \omega \wedge {}^B \tilde{c}_{U\psi} + \sum_{k=1}^N \tilde{c}_{U\psi} \dot{\theta}_k - \frac{1}{2} \omega^T {}^B \tilde{c}_{U\psi} \end{bmatrix} \quad (5)$$

where  $\omega$  is the angular velocity of the system with respect of the inertial system written in the body reference frame,  ${}^B \tilde{c}_{U\psi}$  is the variation of the inertia tensor due to the flexibility (the expression of such term can be found in [15][16]).

### 3.1 Linearized equations

To simplify the control synthesis task for the assembled spacecraft system, the dynamic model in eq. (1) should be linearized around a reference trajectory. However, some considerations have to be reported: the orbital dynamics are assumed to have a negligible effect when the orbital frequency is very low with respect to the attitude controller bandwidth [15][19] (i.e. when the duration of the manoeuvre is short with respect to the orbital period). Furthermore, this study is in line with those space applications, most of the cases, where the spacecraft angular rates are not high enough to retain the gyroscopic stiffness term. In such conditions, which often constitute the standard situation for a satellite orbiting the Earth, the operating point in terms of both attitude and rate, can be assumed equal to zero. Therefore, after having performed a Taylor expansion around the operating point, one obtains

$$\overline{\mathbf{M}}^G \ddot{\mathbf{C}}_T + \overline{\mathbf{C}}_T \dot{\mathbf{C}}_T = \overline{F}_T^G \quad (6)$$

where the overline sign refers to the system written in linearized form. It can be demonstrated [20] that the mass and stiffness matrices correspond to the ones reported in eq. (1), while the damping matrix may be written as

$$\mathbf{C}_T = \begin{bmatrix} \mathbf{0} & \mathbf{0} & \mathbf{0} \\ \mathbf{0} & \mathbf{H}_{jac} & \mathbf{0} \\ \mathbf{0} & \mathbf{0} & 2\Sigma\mathbf{Q} \end{bmatrix} \quad (7)$$

where  $\mathbf{H}_{jac}$  is the Jacobian matrix of the gyroscopic term.

Concerning the kinematics, we describe the non-linear evolution of the attitude motion of the body reference frame with respect to the reference frame by using either Euler's angles or quaternion, as

$$\dot{\mathbf{Q}} = \mathbf{Q} \boldsymbol{\omega} \quad (8)$$

where  $\mathbf{Q}^\theta(\theta)$  is a matrix function of the rotation angles depending on the type of assumed rotation sequence. According to the previous considerations [19], it is possible to assume as the linearization point the zero state of the system, i.e. the satellite in the rest condition, as in

$$\begin{aligned} \mathbf{H}_{jac} &= (\boldsymbol{\omega}^\times)_{\omega=0} {}^B \mathbf{J}_b^G - ({}^B \mathbf{J}_b^G \boldsymbol{\omega}^\times)_{\omega=0} = \mathbf{0} - \mathbf{0} = \mathbf{0} \\ \left. \frac{\partial \mathbf{Q}^\theta(\theta)}{\partial \theta} \right|_{\theta=0} \omega_o \theta + \mathbf{Q}^\theta(\theta_o) (\omega - \omega_o) &= \mathbf{I} \omega \end{aligned} \quad (9)$$

Finally, the linearized equations can be re-arranged in state-space standard form as

$$\begin{aligned} \dot{\mathbf{X}} &= \mathbf{A} \mathbf{X} + \mathbf{B} u \\ \mathbf{Y} &= \mathbf{C} \mathbf{X} + \mathbf{D} u \end{aligned} \quad (10)$$

where

$$\begin{aligned} \mathbf{A} &= \begin{bmatrix} \mathbf{0} & \mathbf{I} \\ -\overline{\mathbf{M}}_T^{-1} \overline{\mathbf{K}}_T & -\overline{\mathbf{M}}_T^{-1} \overline{\mathbf{C}}_T \end{bmatrix} \\ \mathbf{B} &= [\mathbf{0} \quad \mathbf{B}_v]^T \quad \mathbf{C} = [\mathbf{C}_{ox} \quad \mathbf{C}_{ov}] \end{aligned} \quad (11)$$

and  $\mathbf{D}$  feedthrough term. The matrix  $\mathbf{B}_v$  is defined as

$$\mathbf{B}_v = \begin{bmatrix} \mathbf{I} & \mathbf{0} & \mathbf{0} \\ \mathbf{0} & \mathbf{I} & \mathbf{0} \\ \mathbf{0} & \mathbf{0} & \mathbf{B}_m \end{bmatrix} \quad (12)$$

Assuming the flexible structure is not subjected to forces other than the actuators actions, the input forces  $u$  will include  $u = [f_G, c_G, \psi]$  and the matrix  $\mathbf{B}_m = \tilde{\mathbf{K}}_{U\psi}$ . In case of collocated devices,  $\mathbf{C}_{ox} = \mathbf{0}, \mathbf{C}_{ov} = \mathbf{B}_v^T$ .

### 3.2 Spacecraft model

The satellite is composed of a flexible appendage attached to a rigid platform in correspondence of an attachment point  $P_1$  defined in the S/C reference frame, whose origin is located at the centre of the launch vehicle payload adapter (see Fig. 3). The inertial properties of the platform, without considering the appendage, are listed in Table 3.

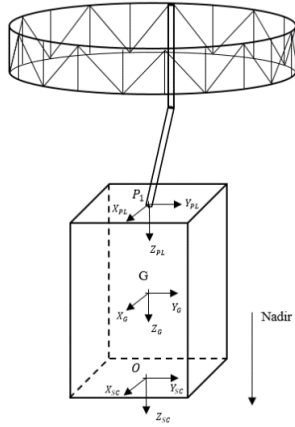


Fig. 3. Schematic of the spacecraft equipped with a large flexible mesh reflector

Table 3. Platform inertial properties

Mass (kg)	Inertia (kg/m <sup>2</sup> )						CoG (m)		
	J <sub>xx</sub>	J <sub>yy</sub>	J <sub>zz</sub>	J <sub>xy</sub>	J <sub>xz</sub>	J <sub>yz</sub>	X	Y	Z
940	590	620	550	2	4	-8	0	0	-1

For control purposes, it is often convenient to retain in the dynamic model the elastic modes computed at specific locations of the flexible structure. Such points are identified with specific nodes in the FEM model of the flexible appendage, namely Nodes of Interest (NOIs). In this paper, two sets of NOIs are proposed. The first group of nodes, named Requirements NOIs (R-NOIs), aims at monitoring elastic displacements to check if the system requirements are satisfied when performing attitude manoeuvres. The second sub-set, named Distributed-control NOIs (D-NOIs), includes those nodes where the active vibration control distributed system exerts its control actions, as indicated in Fig. 4. Therefore, the elastic modes of the structure, used to project the forces of actuators on the appendage modal base, will be computed in such distinct locations, thus reducing the size of the inputs to the model. Among the Requirements NOIs, the nodes of the center phase of the antenna and the reflector tip are considered to evaluate the maximum allowed displacement for the antenna reflector (see Fig. 4).

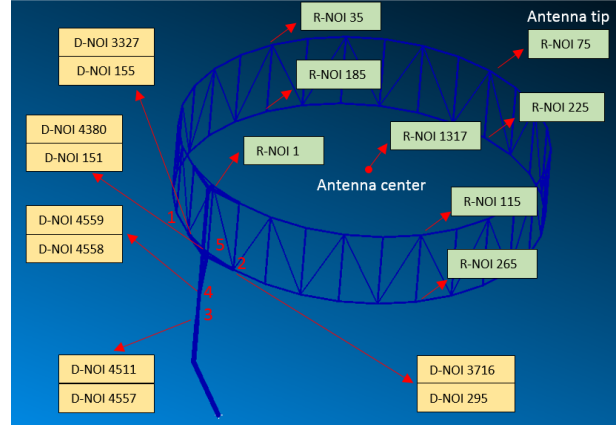


Fig. 4. Requirements and Distributed-control NOIs

#### 4. General placement strategy

In this section a general procedure to perform a straightforward and computationally efficient placement for high-dimensional structures is proposed and tested on the study case in Par. 2. In detail, two methodologies are contemplated to carry out in parallel the placement of a set of actuators and sensors on a flexible structure and to compare their outcome for validation:

- A *Norm-based placement* method makes use of the controllability and observability gramians of the system and attempt to optimize the sensor and actuator locations to increase, from a control perspective, the relative controllability and observability of the important system mode;
- A *MSE|SVD-based placement* method is based on the extraction of the Modal Strain Energy (MSE) from a commercial finite element tool and on the successive computation of Singular Values (SVDs) of the modal input matrix of the system to evaluate the effect of positioning collocated devices on flexible structures.

##### 4.1 Problem set-up

Let us consider placing  $S$  collocated actuators and sensors on a flexible structure. The devices are assumed to be implemented between two adjacent nodes  $m, n$  of the structure, each node with six degrees of freedom  $V_{nm}$

$$V_{nm} = [u_m, v_m, w_m, \alpha_m, \beta_m, \theta_m, u_n, v_n, w_n, \alpha_n, \beta_n, \theta_n] \quad (13)$$

where  $u, v, w$  indicate the translational degrees of freedom along the local X, Y and Z-axis, while  $\alpha, \beta, \theta$  the rotational ones. Generally, [21], the effect of a smart device on a flexible structure can be described in terms of forces and torques applied (or displacements and rotations sensed) on specific nodes of its finite element model by means of an electromechanical coupling term  $\mathbf{K}_{U^e}^e$ . Such term will depend on both specific properties of the device and a mapping matrix distributing the exerted generalized forces (sensed variables) on the

degrees of freedom of the nodes of the structure as listed in the vector below

$$\mathbf{K}_{U\Psi}^e = [0, \dots, 0, F_X^m, F_Y^m, F_Z^m, C_X^m, C_Y^m, C_Z^m, \dots, 0, F_X^n, F_Y^n, F_Z^n, C_X^n, C_Y^n, C_Z^n, \dots, 0]^T \quad (14)$$

where  $F_X, F_Y, F_Z$  and  $C_X, C_Y, C_Z$  are the terms regrouping the active material properties variables which, multiplied by an input voltage  $\Psi$  vector in case of piezoelectric devices, will produce effective forces and torques on the nodes  $m, n$  of the structure (or will define which variables the sensor is able to perceive). This vector has length equal to the number of the total degrees of freedom of the finite element system and the only non-zero elements are those corresponding to the translational and rotational degrees of freedom of the nodes where the device is implemented.

In this paper, a  $\pi$ -shaped Piezoelectric Stack Actuator (PPSA) mounted on two L-support mechanical frames at a certain distance from the surface of the element is considered [18], in order to observe the effects of applying both axial forces and bending moments. In this case, eq. (14) can be rewritten as

$$\mathbf{K}_{U\Psi}^e = c_{PZ} [0, \dots, 1, 0, 0, 0, 0, -h_a, -1, 0, 0, 0, 0, h_a, \dots, 0]^T \quad (15)$$

with  $h_a$  offset between the longitudinal axis of the piezoelectric stack and the neutral plane of the passive structure and

$$c_{PZ} = n \frac{d_{33} A_{PZ} E_{PZ}}{l_{PZ}} \quad (16)$$

where  $d_{33}$  is the piezoelectric material coefficient,  $n$  is the number of layers composing the piezo-stack,  $A_{PZ}$ ,  $E_{PZ}$  and  $l_{PZ}$  are the area, the Young module and the length of the device respectively. Furthermore, a rotation matrix  $\mathbf{T}_{g \leftarrow e}$  is needed to transfer the actions of the device from an element local frame to the global frame of the assembled finite element model, as indicated below

$$\mathbf{K}_{U\Psi}^g = \mathbf{T}_{g \leftarrow e} \mathbf{K}_{U\Psi}^e \quad (17)$$

where  $\mathbf{T}_{g \leftarrow e} = \mathbf{R}_3(\theta_x) \mathbf{R}_2(\theta_y) \mathbf{R}_1(\theta_z)$ . In detail, the first two rotations are needed to define the position of the element in the tri-dimensional space, while the third rotation is required when assuming that the element section may be oriented in different ways around the longitudinal axis of the element. This approach is proposed in the placement process to represent different orientations of the actuators (see Fig. 5). In case of placing PPSA actuators, the generated bending moment can be generally oriented with respect to the three coordinated axes X, Y and Z. Therefore, their efficacy in suppressing vibrations depends not only on their actual location on the structure, but also on how the designer decides to orient them in the 3D space. Such an

issue has been here addressed in the placement procedure by enlarging the initial set of possible physical locations (corresponding to the actual finite elements of the structure) with additional virtual locations (i.e. different orientations of the devices on a same finite element). In this case, for each physical location, four different orientations of the piezo stack have been considered (in black in Fig. 5, while in green the longitudinal forces and in red the actual device). It should be noticed that the enlarged dataset is further used to carry out the placement process.

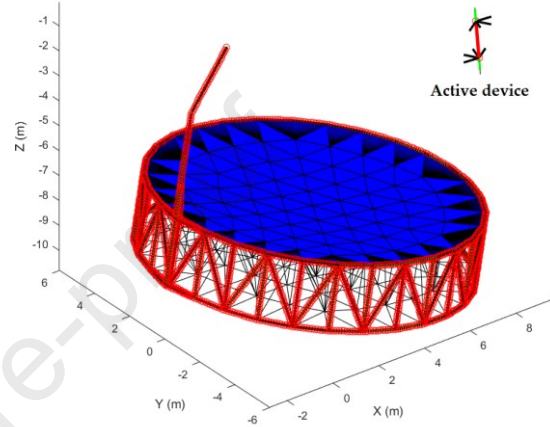


Fig. 5. Set of possible locations of smart devices

In detail, a location  $s = [ID | E_{ID} | N_{ID} | O_r]$  is defined by a label  $ID$ , by the identification number  $E_{ID}$  of the finite element where the active device is implemented, by a vector  $N_{ID}$  listing the IDs of the two considered nodes, and by a term  $O_r$  indicating the distinct orientation of the active device (e.g. the virtual location). The complete set of locations is portrayed in Fig. 5. Finally, the physical input matrix  $\mathbf{B}$  is column-wise assembled by horizontally concatenating all the  $B_i, i=1, \dots, S$  vectors, one for each considered device, as in

$$\mathbf{B} = [B_1 \quad B_2 \quad \dots \quad B_S] \quad (18)$$

Then, the modal input matrix is defined by pre-multiplying such matrix by the modes as in

$$\mathbf{B}_m = \Phi^T \mathbf{B} \quad (19)$$

where  $\Phi$  is the matrix containing the elastic modes of the flexible structure. Furthermore, in case of collocated system the modal output matrix  $\mathbf{C}_m$  is assumed equal to the transpose of  $\mathbf{B}_m$ .

#### 4.2 Norm-based

The first method relies on the definition of system norms, based on controllability and observability gramians, to investigate the placement of co-located pairs of actuators/sensors on large flexible structures

[22]. A placement index grading the effects of an actuator/sensor on a specific mode is defined by considering the ratio between the transfer function of the  $i$ -th mode and  $k$ -th actuator  $\|G_{ki}\|_\infty$  and the transfer function of the structure with all the actuators candidates  $\|G\|_\infty$ .

$$\sigma_{\infty ki} = w_{ki} \frac{\|G_{ki}\|_\infty}{\|G\|_\infty}, \quad k = 1, \dots, \mathcal{R}, \quad i = 1, \dots, n \quad (20)$$

where  $w_{ki} \geq 0$  are weights that can be included to selectively give more importance to a specific actuator or mode in practical applications, as for multiple modes control it is generally not possible to find locations which are optimal for all the modes. In detail, based on the hypothesis of small damping [22], which is often the case for a spacecraft flexible appendage flexible structure, an approximated expression for the transfer functions in eq. (20) may be derived as

$$\|G_{ki}\|_\infty \cong \frac{\|B_{mki}\|_\infty \|C_{mi}\|_\infty}{2\xi_i \omega_i} \quad (21)$$

$$\|G\|_\infty \cong \sqrt{\sum_{k=1}^R \|G_k\|_\infty^2} \quad (22)$$

with

$$\|G_i\|_\infty \cong \sqrt{\sum_{k=1}^R \|G_{ki}\|_\infty^2}, \quad i = 1, \dots, N \quad (23)$$

The placement indexes  $\sigma_{2ki}$  can be rearranged in a matrix  $\Lambda_\infty$  as follows

$$\Lambda_\infty = \begin{bmatrix} \sigma_{\infty 11} & \sigma_{\infty 12} & \cdots & \cdots & \cdots & \cdots & \cdots \\ \sigma_{\infty 21} & \sigma_{\infty 22} & \cdots & \cdots & \cdots & \cdots & \cdots \\ \cdots & \cdots & \cdots & \cdots & \cdots & \cdots & \cdots \\ \sigma_{\infty i1} & \sigma_{\infty i2} & \cdots & \cdots & \cdots & \cdots & \cdots \\ \cdots & \cdots & \cdots & \cdots & \cdots & \cdots & \cdots \\ \sigma_{\infty n1} & \sigma_{\infty n2} & \cdots & \cdots & \cdots & \cdots & \cdots \end{bmatrix} \quad (24)$$

As it can be deduced by directly inspecting eq. (24), the  $k$ -th column of the matrix lists the indices evaluating the effect of the  $k$ -th actuators on all the modes of the structure. Conversely, the  $i$ -th row of the matrix regroups the indices of the  $i$ -th mode for all the considered actuators. Therefore, a vector comprising the actuators placement indices can be defined as

$$\sigma_a = [\sigma_{a1} \quad \sigma_{a2} \quad \cdots \quad \cdots] \quad (25)$$

where each  $k$ -th element is

$$\sigma_{ak} = \max_i (\sigma_{ik}), \quad i = 1, \dots, n, \quad k = 1, \dots, S \quad (26)$$

The vector  $\sigma_{ak}$  provides the designer with a significant information: it quantifies the weighted contribution of the  $k$ -th actuator at all the (selected) modes to the norm of the flexible structure. With this in mind, the actuators related to small values of placement indexes can be removed being the least significant ones.

$$\sigma_{OPT} = \max_k (\sigma_a) \quad k = 1, \dots, S \quad (27)$$

By placing the actuator and sensor at the locations of the maximum index values, the vibration of the  $i$ -th mode is controlled by an actuator input signal of minimal energy and measured by a sensor with maximum output energy.

#### 4.3 MSE|SVD-based

The placement of active elements in a flexible structure can be carried out from the inspection of the map of the Modal Strain Energy (MSE) in the finite element model. The element strain energy is defined as the amount of elastic energy stored in a finite element, as follows

$$ESE_e = \frac{1}{2} u_e^T \mathbf{K}_{ee} u_e \quad (28)$$

where  $u_e$  is the element displacement and  $\mathbf{K}_{ee}$  is the stiffness matrix. The active parts should be placed where their authority over the modes to control is the largest. Indeed, according to [22], the control authority is proportional to the fraction of MSE in the element. The search procedure is greatly assisted by the fact the map of the fraction of MSE is directly available in commercial finite element packages (such as MSC Nastran). The map of modal strain energies is useful to initially discriminate best locations, but it does not provide enough practical information on how to implement actuators on the structure. Indeed, the actuators may be mounted in different orientations on a same finite element (especially when referring to a piezo stack with offset on a truss structure). To consider also different orientations and generally to reduce the set of best locations where to place the actuator/sensor, the minimization of the maximal physical control force is here chosen as the criterion to drive the actuator placement [23]. Furthermore, the latter method is suitable to be used in conjunction with the MSE approach. Indeed, the physical control force strategy is based on considering all the possible combinations of collocated actuators/sensors to compose the modal input matrix, thus leading to high computational costs, which can be reduced by choosing a proper subset of possible location thanks to MSE information. In this context, the Singular Value Decomposition (SVD) of the input matrix is used to measure the system controllability as follows

$$\mathbf{B}_m = \mathbf{U} \mathbf{S}_v \mathbf{Q} \quad (29)$$

$$\mathbf{S}_v = \begin{bmatrix} \boldsymbol{\Sigma} & \mathbf{0} \\ \mathbf{0} & \mathbf{0} \end{bmatrix}, \quad \boldsymbol{\Sigma} = \text{diag}[\sigma_1, \dots, \sigma_m]$$

Where  $\sigma_i$  is a singular value of the matrix  $\mathbf{B}_m$ . Indeed, it can be demonstrated [23] that the physical input force  $u_i^*$  is proportional to the modal force  $f_{Ci}^*$  and inversely proportional to the singular value  $\sigma_i$  as indicated below



$$u_i^* = \frac{f_{Ci}^*}{\sigma_i} \quad (30)$$

Therefore, if the minimal singular value of a matrix  $\mathbf{B}_m$  is larger, the maximal physical control force will be smaller. Finally, the optimization objective function may be formulated as follows

$$\max [\sigma(\mathbf{B}_m)_{\min}] \quad (31)$$

The proposed placement approach is described by following some steps:

- Define initial subsets  $U_i$ , where  $i=1:N$  number of considered modes, listing prospective locations identified by MSE data referred to the  $i$ -th mode;
- Compute combinations  $c_i$  of the locations for a  $i$ -th mode included in each subset  $U_i$ , taken  $\varepsilon_i$  times without repetitions, where  $\varepsilon_i$  is the number of collocated devices chosen to control/sense a mode at a time;
- Also consider combinations  $C_i = \prod_i c_i$  among different  $U_i$  sets to simultaneously control more than one mode. Such combinations are then used as hint to assemble  $C_i$  distinct input matrices  $\mathbf{B}$  in a column-wise fashion, where each column indicates the effect of one device on the flexible structure;
- Calculate the SVs of the input matrices  $\mathbf{B}_m = \Phi^T \mathbf{B}$  of all the combinations, and the optimal combination should be the one that meet the objective function in eq. (31).

#### 4.4 General placement strategy implementation

Information from finite element software generally contains positions and ID of the nodes, Modal Strain Energy tables as well as Property Sets (PSETs) associated to different parts of the model, comprising characteristics as material association and dimensions of the component. In this context, two methods have been contemplated to automatically choose specific finite elements for placement purposes based on different inputs (see Fig. 6). The first approach identifies one or more volumes of interest; it may be used when only specific zones of the flexible appendage are available to practically implement active vibration devices. The second method selects particular PSETs associated to precise features, as plates or beam elements, useful when investigating the placement of devices on a structure composed of multiple types of finite elements.

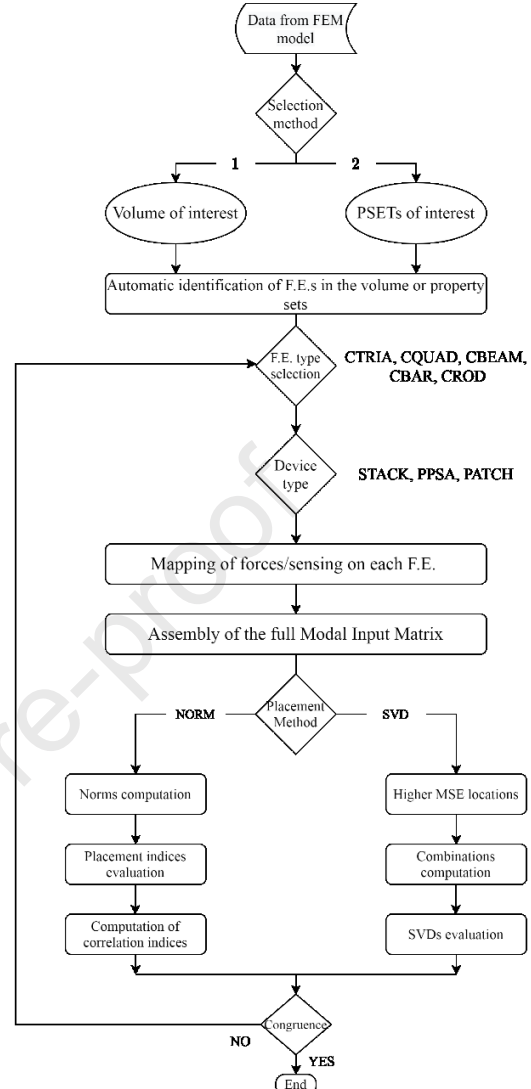


Fig. 6. General workflow of the placement procedure

After having identified the elements of interest according to one of the two methods, one may want to further select a type of finite element to carry out the placement procedure. The accounted categories are five, namely CQUAD, CTRIA, CROD, CBAR and CBEAM elements, thus allowing to cover for a wide range of designs of flexible structures. Once defined the final set of finite element to be taken into account, the characteristics of actuators/sensors can be selected, choosing among the piezoelectric stacks, patches and stack with offset (as in this study case). At this point, the action of the device is mapped onto the structure as previously illustrated. The *full-assembled* Modal Input Matrix  $\mathbf{B}_m$  is then computed: it contains all the possible locations selected so far for placement purposes. The two open-loop methods are then applied.

Finally, the results deriving from the two procedures are compared in terms of set of identified optimal locations to verify the output of the procedure. An overview of the placement algorithm is portrayed in Fig. 6.

4.5 Results

The plot of the placement matrices  $\sigma_{\infty ki}$  for the first, second, third and fourth mode are represented in Fig. 7 and Fig. 8, where the peaks of the placement indexes (both higher value and second higher peak) are circled in red. Indeed, frequencies up to 3 Hz have been considered for the placement, as it may interfere with the bandwidth of the controller and cause control/structure interaction issues. Higher frequencies have been discarded as it is less likely they may provoke performance deterioration. The outcome is further summarized in Table 4.

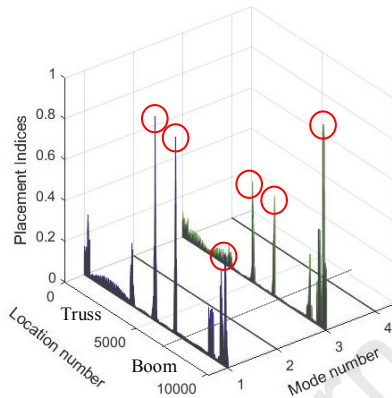


Fig. 7. Placement indices for  $i=1:4$  with  $w_{k1,3} = 1$  and  $w_{k2,4} = 0$

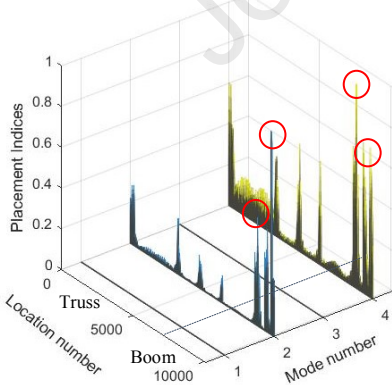


Fig. 8. Placement indices for  $i=1:4$  with  $w_{k2,4} = 1$  and  $w_{k1,3} = 0$

	(9927)	F: $\pm Z$ , M: $\pm X$	(0.55)
2	(9925)	F: $\pm Z$ , M: $\pm Y$	(1)
	(8977)	F: $\pm Z$ , M: $\pm Y$	(0.58)
3	(9927)	F: $\pm Z$ , M: $\pm X$	(1)
	(4924,6480)	F: $\pm Y$ , M: $\pm XZ$	(0.57,0.58)
4	(8977)	F: $\pm Z$ , M: $\pm Y$	(1)
	(9481)	F: $\pm Z$ , M: $\pm Y$	(0.74)

It may be noticed how the axes of the bending moments exerted by the devices are oriented as expected with respect to the directions of the bending modes. Indeed, the first mode is composed mainly of a bending about the Z-axis and a minor bending about the X-axis. The second mode is a bending about the Y-axis, the third mode is a torsion of the reflector about the X-axis and consequent bending of the boom with respect to the same axis. The fourth mode is similar to the second, being again a bending about the Y-axis, where the boom deflects as the second mode of a constrained-free beam.

As far as the second placement method is concerned, the MSE data are extracted from MSC Nastran and imported in Matlab environment for further processing.

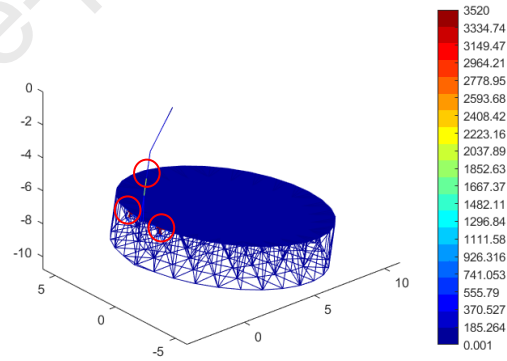


Fig. 9. MSE (element density) for the first mode

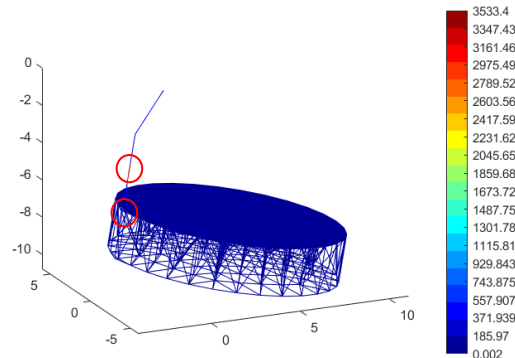


Fig. 10. MSE (element density) for the second mode

Table 4. Norm-based placement outcome

Mode	Location ID	Forces direction: F. Force, M. Moment	Placement Index
1	(4975,6426)	F: $\pm Y$ , M: $\pm XZ$	(1,0.98)

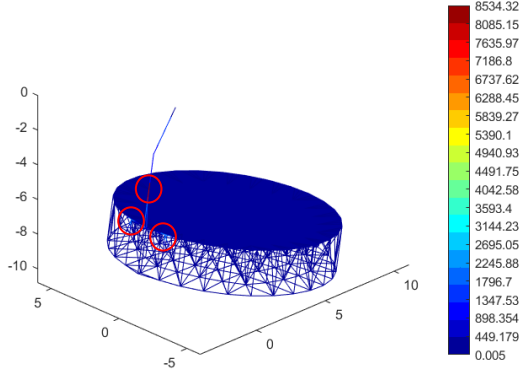


Fig. 11. MSE (element density) for the third mode

The MSE in terms of energy density (weighted accordingly to the effective dimension of the finite element, for a more accurate information about the energy distribution) is reported in Fig. 10 to Fig. 13. It can be noticed a good correspondence between elements with higher energy and results from the previous placement method.

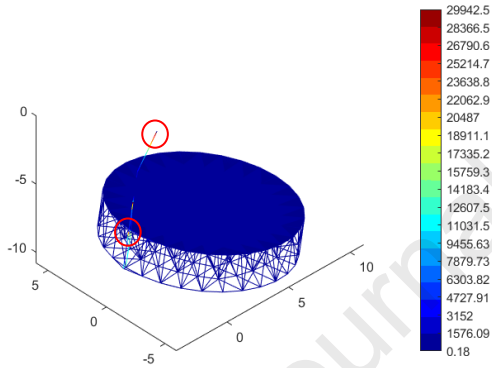


Fig. 12. MSE (element density) for the fourth mode

After having identified elements in the subsets  $U_i$ , possible combinations are computed as indicated in Par. 3.3. The results are summarized in Table 5. In detail, combinations of two actuators for each mode have been considered ( $\varepsilon_i = 2$ ).

Table 5. MSE|SVD-based placement outcome

Mode	Locations ID	Normalized $\sigma(\mathbf{B}_m) _{\min}$
1-3	[4975,6426 9927, 8977]	(1)
	[4974,6426 9935, 8977]	(0.99)
2-4	[9925, 8977 8977, 9841]	(1)
	[9926, 8977 8977, 9841]	(0.97)

A good correspondence is evident when considering the results of the previous method. In the next section, the final configuration is presented based on such results.

#### 4.6 Final configuration

In the proposed configuration, a total of five actuators are placed on the flexible structure, in correspondence of the locations with higher placement indices and minimum SV for each considered mode. It is interesting to note that the devices are effective, in different amounts, on more than one mode at a time (see Table 6).

Table 6. Outcome summary

Act/ Sens	Element ID	Mode			
		1	2	3	4
1	2907	++	-	+	-
2	3270	++	-	+	-
3	4077	-	++	-	+
4	4079	+	-	++	
5	3908	-	+	-	++

++ very effective, + effective, - not effective

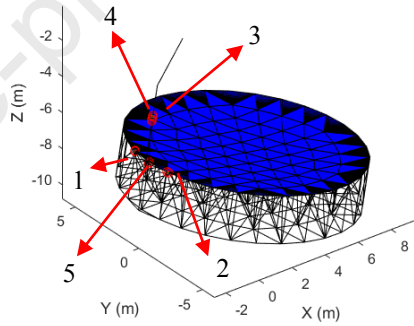


Fig. 13. Final configuration of co-located actuators/sensors

The position and related number of the actuators is depicted in Fig. 13.

### 5. Robust Control synthesis and design

This section begins with a summary of the necessary models for the description and analysis of uncertain Linear Time Invariant (LTI) systems; following, after a brief introduction of the  $\mu$ -synthesis control approach, an attitude control accounting for attitude (angles and angular rates) measurements, coupled with a vibration controller using measurements obtained via piezoelectric sensors, is proposed based on this method.

#### 5.1 Uncertain modelling

Any real system is characterized by unwanted uncertainties, coming from neglected dynamics in the modelling phase, non-linearities and unknown parameters, which can significantly affect the stability and performance of the system. The various source of uncertainties mentioned above may be grouped in two main classes: structured uncertainties, which are related to changes in actual parameters, and unstructured

uncertainties which, instead, are frequency dependent and are generally used to describe some unmodelled dynamics.

A Linear Fractional Transformation (LFT) modelling strategy [24] is hereby adopted since it provides a unified method to gather and isolate all the uncertainties of the dynamical model; in fact, denoted  $G$  as a generic uncertain process, it is possible to express it as a feedback interconnection of a nominal plant  $M$  and a block-diagonal matrix  $\Delta = \text{diag}(\Delta_i)$  with  $\|\Delta\|_\infty \leq 1$  as sketched in Fig. 14.

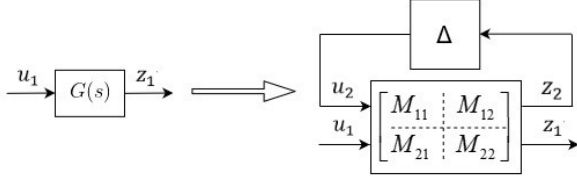


Fig. 14. LFT representation of an uncertain system

In this formulation,  $G$  is then expressed by the upper-LFT of  $M$  with  $\Delta$  as follows:

$$G = F_u(M, \Delta) = M_{22} + M_{21}\Delta(I - M_{11}\Delta)^{-1}M_{12} \quad (32)$$

With respect to the dynamical model derived in Section 3, Table 7 reports the uncertain parameters considered in the plant and the relevant extent of perturbations; uncertainties in the translational and rotational modal participation factors and damping values have been neglected with respect to the other parameters in order to keep the complexity of the LFT system as low as possible. It has to be, in fact, noted that high order LFTs, together with the presence of highly packed and lightly damped flexible modes can significantly complicate the computation of precise lower and upper bound of  $\mu$  [25]. Furthermore, to keep the model as close as possible to the reality and to avoid possibly conservative results in the synthesis, the uncertainty on the diagonal elements of the inertia tensor is considered linearly proportional to the mass.

Table 7. Uncertain parameters of the plant

	Uncertainty
Mass	5 % of N.V.
$[J_{xx}, J_{yy}, J_{zz}]$	f(Mass)
$[J_{xy}, J_{yz}, J_{xz}]$	5 % of N.V.
Natural frequencies	5 % of N.V. (for the first 5 modes)
$c_{pz}$	15 % of N.V.

### 5.2 Plant structure for robust control design

Robust control methods aims at designing a fixed controller such that some defined levels of performance (i.e. reference tracking, disturbance rejection and noise

attenuation) and stability margins of the closed loop system are guaranteed, irrespective of the change in the plant dynamics over a predefined range of uncertainties. The proposed synthesis model used to design the controllers is presented in Fig. 15.

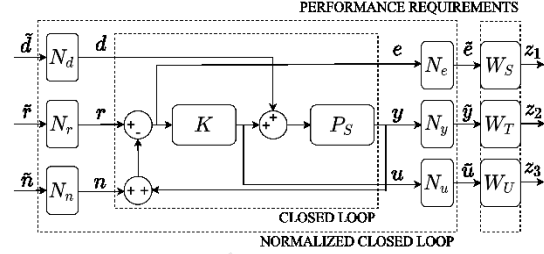


Fig. 15. Synthesis model

where:

- closed loop inputs  $d, r, n$  indicates respectively the external disturbance, reference signal and measurement noise vectors and  $\tilde{d}, \tilde{r}, \tilde{n}$  are their normalized counterparts via the scaling functions  $N_d, N_r, N_n$ ;
- the closed loop outputs  $e, y, u$  are respectively the error signal  $e = r - y - n$ , measured output and control signals vectors and  $\tilde{e}, \tilde{y}, \tilde{u}$  are their normalized counterparts via the scaling functions  $N_e, N_y, N_u$ ;
- the performance outputs  $z_1, z_2, z_3$ .

The input-output map of the synthesis model in Fig. 15 is represented as follows

$$\begin{bmatrix} z_1 \\ z_2 \\ z_3 \end{bmatrix} = \begin{bmatrix} W_S & 0 & 0 \\ 0 & W_T & 0 \\ 0 & 0 & W_U \end{bmatrix} \begin{bmatrix} -N_e S P_S N_d & N_e S N_r & -N_e S N_n \\ N_y S P_S N_d & N_y T N_r & -N_y T N_n \\ -N_u T_o N_d & N_u S_o K N_r & -N_u S_o K N_n \end{bmatrix} \begin{bmatrix} \tilde{d} \\ \tilde{r} \\ \tilde{n} \end{bmatrix} \quad (33)$$

with

$$S = (I + P_S K)^{-1} \quad T = I - S \quad (34)$$

$$S_0 = (I + K P_S)^{-1} \quad T_0 = I - S_0$$

Finally, the weighting functions  $w_s, w_r, w_u$  are used to define the control design requirements by shaping the sensitivity function, the complementary sensitivity function and control sensitivity transfer function. In this study, a diagonal structure is selected for all weighting functions as follows [26]

$$w_s^{(ii)}(s) = \left( \frac{s}{n \sqrt{M_s^{(i)}} + \omega_s^{(i)}} + \omega_s^{(i)} \right)^n, \quad w_T^{(ii)}(s) = \left( \frac{s + \omega_T^{(i)} \sqrt{A_T^{(i)}}}{n \sqrt{M_T^{(i)}} + \omega_T^{(i)}} \right)^n \quad (35)$$

$$W_U^{(ii)}(s) = \left( \frac{\frac{s}{\sqrt[n]{M_U^{(i)}}} + \omega_U^{(i)}}{\frac{s}{\sqrt[n]{A_U^{(i)}}} + \omega_U^{(i)}} \right)^n \quad (36)$$

where the parameters  $M_{\{S,T,U\}}^{(i)}, A_{\{S,T,U\}}^{(i)}, \omega_{\{S,T,U\}}^{(i)}$  are properly selected and tuneable quantities used to impose the required closed loop behaviour.

By shaping the sensitivity function  $S(s)$ , the weighting function  $w_s(s)$  allows to define the following requirements:

- A minimum bandwidth of the closed loop system to satisfy minimum rise time requirements ( $\omega_{cl} > \omega_S$ );
- A desired maximum overshoot of the response (generally below 30%) by constraining accordingly a value of the maximum peak of the sensitivity function via  $M_S$ ;
- Some desired steady state tracking error performance by constraining the lower frequency gain of the sensitivity function under  $A_S$ .

Similar considerations are valid for  $w_T$  used to shape the complementary sensitivity function, which is a good indicator of the system response to reference and sensor noise inputs, and the weighting function  $w_U$ , which is designed to shape the frequency behaviour of the control signal. Indeed, the objective of the function  $w_U$  is to limit the control signal and to guarantee compatibility with actuation capabilities (for example, to avoid actuator saturation due to bandwidth limitation).

### 5.3 $\mu$ -synthesis control design

For the current problem, which presents mostly structured uncertainties (i.e. mass, inertia tensor, natural frequencies, etc.),  $H_\infty$  control methods are discarded since they cannot tackle well huge structured  $\Delta$  block without producing additional conservativeness in the model and severely undermining the performance of the closed loop. Therefore,  $\mu$ -synthesis, although more computationally problematic, is selected for the current study. Basically, the  $\mu$ -framework introduces a new metric based on the Structured Singular Value  $\mu$  [27]. By assuming that  $\Delta$  belongs to the set:

$$\underline{\Delta} = \left\{ \text{diag}(\delta_1 I_{r_1}, \dots, \delta_s I_{r_s}, \Delta_1, \dots, \Delta_k) : \delta_i \in \mathbb{C}, \Delta_j \in \mathbb{C}^{n_j \times n_j} \right\} \quad (37)$$

with  $\bar{\sigma}(\Delta) \leq 1, \forall \Delta \in \underline{\Delta}$ , then given a matrix  $M \in \mathbb{C}^{n \times n}$ , the structured singular value  $\mu(M)$  is defined as:

$$\mu(M) = \frac{1}{\min(\bar{\sigma}(\Delta) : \Delta \in \underline{\Delta}, \det(I + M\Delta) = 0)} \quad (38)$$

unless no  $\Delta \in \underline{\Delta}$  makes  $I + M\Delta$  singular, then  $\mu(M) = 0$ . Therefore,  $\mu(M)$  is the inverse of the smallest perturbation (in terms of  $\bar{\sigma}(\Delta)$ ) among all possible  $\Delta \in \underline{\Delta}$ .

The plant scheme proposed in Fig. 15 can be rearranged in the LFT framework as in Fig. 16 with  $K$  the controller and  $P_e$  the generalized plant, also containing the weighting and scaling functions previously introduced.

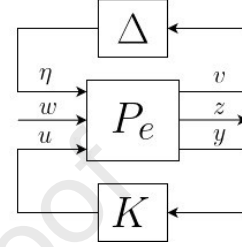


Fig. 16. LFT representation of a general control scheme

The synthesis problem to be solved is, then, the following:

Find a controller  $K$  such that it minimizes

$$\inf_K \sup_{\omega} \mu(F_l(P_e(j\omega), K(j\omega)))$$

where  $F_l(P_e, K)$  is the lower LFT of the generalized plant with the controller.

At present, there is still no direct method to synthesize the controller directly on the optimization of the  $\mu$  and a solution can only be found iteratively (D-K iteration) if the  $\mu$  is replaced by a mildly conservative upper bound. Since the joint convexity over the variable  $K$  (controller) and  $D$  (scaling matrix) is not guaranteed, the iteration may converge to a local minimum [28].

## 6. Simulations and Results

In this section, the results of the control synthesis procedure are reported. In addition, the synthesized robust controller  $K$  and an in parallel Proportional-Derivative feedback vibration controller  $K_v$  are tested in a simulator taking into account the dynamic nonlinearities presented in Par. 3, as indicated in Fig. 17, where the term  $P_{NN}$  indicates the non-linear plant.

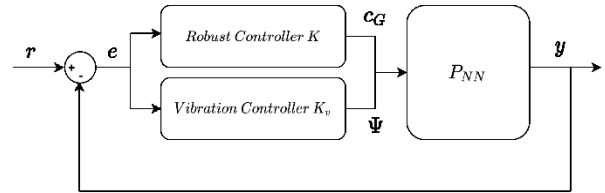


Fig. 17. Robust attitude and PD-feedback vibration control scheme

### 6.1 Results of the $\mu$ -synthesis control design

The main results concerning the synthesis of the attitude robust controller are reported in this section. In detail, Fig. 18 reports upper and lower bounds on the structural singular value for the attitude controller obtained via  $\mu$ -synthesis.

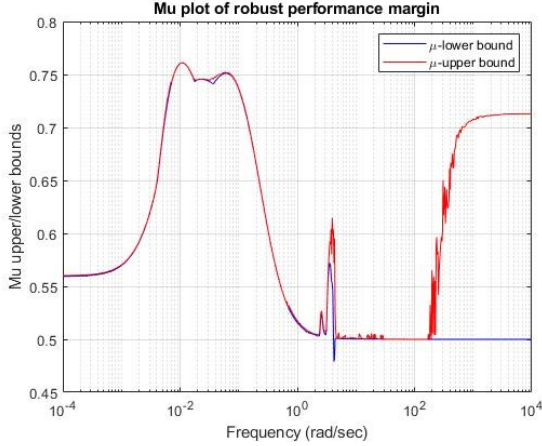


Fig. 18. Robust performance margin

It is shown that the system satisfies the performance requirements with a sufficient margin of value 0.761 obtained at a frequency of 0.01 rad/s.

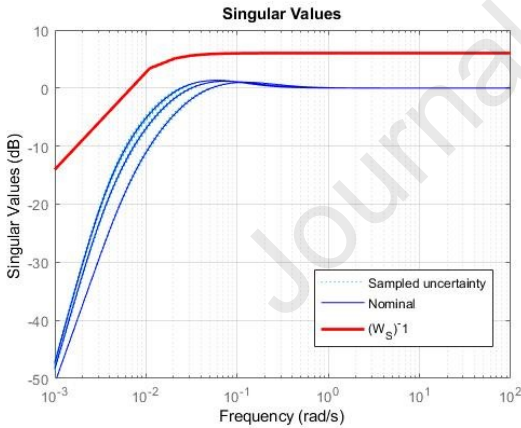


Fig. 19. Singular Values of the sensitivity function

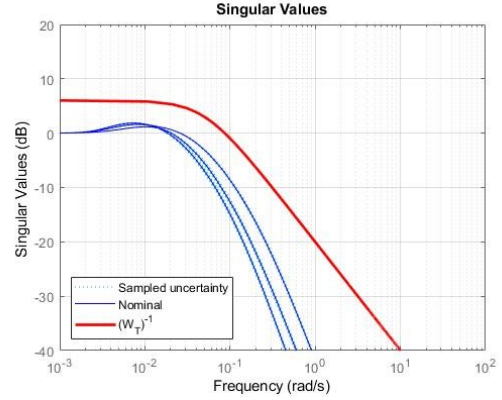


Fig. 20. Singular Values of the complementary sensitivity function

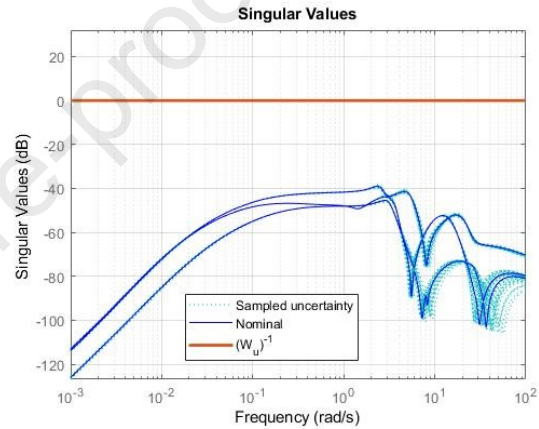


Fig. 21. Singular Values of the control sensitivity function

Furthermore, Fig. 19 to Fig. 21 show respectively the singular values of the sensitivity function, complementary sensitivity function and command function for the scaled closed loop system compared with the inverse of the performance weighting function  $W_S, W_T, W_U$ .

### 5.3 Results of non-linear simulator

The main results deriving from implementing the controller in the simulator implementing the non-linear equations of motion are reported in Fig. 22 to Fig. 26. In detail, Fig. 22 depicts the time histories of the actual Euler's angles (in blue). In detail, a set-point reference equal to [30,20,10] degrees is provided to the attitude controller. The system shows a maximum overshoot under the set constraints in the synthesis process (below 30%,  $M_S = 2$ ). The constraint on maximum steady state error is respected too, being equal to  $0.001e_M$ , where  $e_M$  is the maximum expected error with respect to the reference.

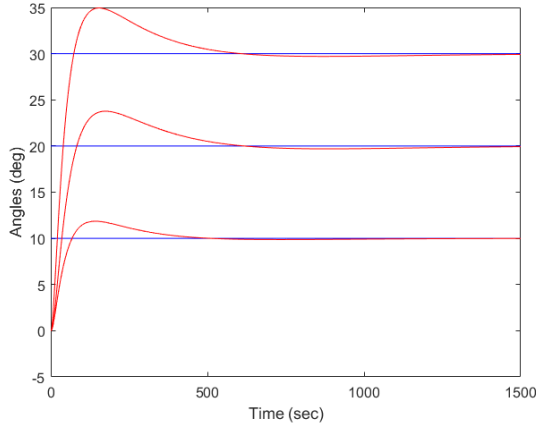


Fig. 22. Time histories of Euler's angles (in blue: set point reference, in red: actual angles)

The time histories of the torques  $c_G$  are illustrated in Fig. 23. The maximum torque is below the saturation constraint imposed to the robust controller during synthesis iterative process.

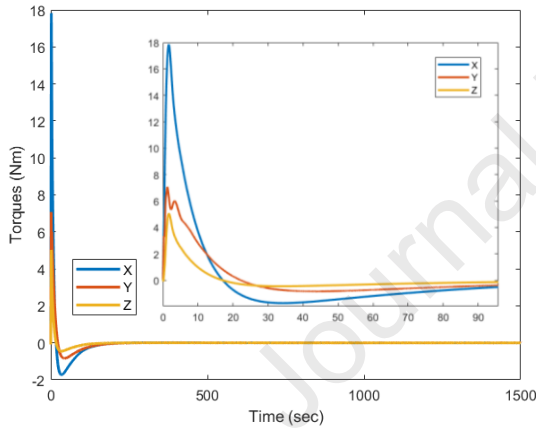


Fig. 23. Torques time histories (with zoom on the first 100 seconds)

In Fig. 24, the displacement of the tip of the antenna with respect to time is reported. The vibration system ensure the maximum displacement is in a sub-millimetre range, suitable to perform high precision pointing operations.

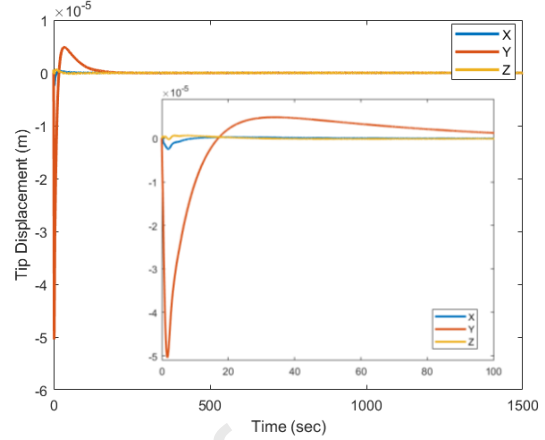


Fig. 24. Tip displacement time history (with zoom on the first 100 seconds)

Finally, both the results from sensing and actuation by using smart piezoelectric actuators and sensors are portrayed in Fig. 25 and Fig. 26. The values of voltages required to the devices to perform the vibration suppression are both in the range of commercially available products.

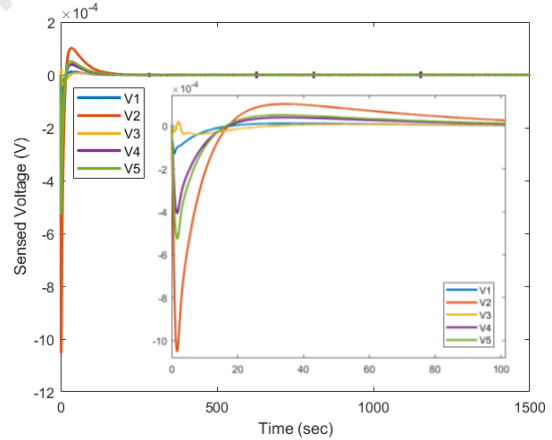


Fig. 25. Sensed voltage time histories (with zoom on the first 100 seconds)

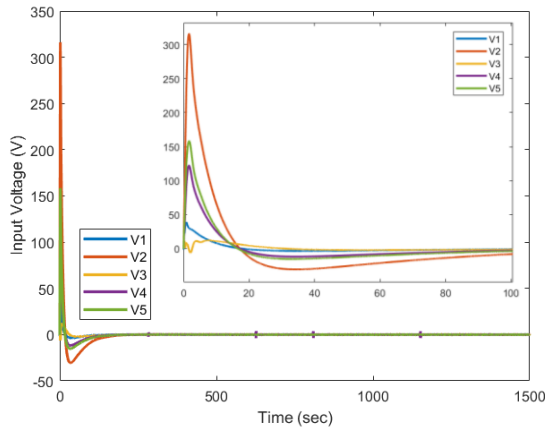


Fig. 26. Input Voltages time histories (with zoom on the first 100 seconds)

## 7. Conclusions

In this paper, a general architecture to perform end-to-end design of an in parallel robust attitude control and vibration suppression system is presented. To test the proposed methodology, a Large Mesh Reflector Model (LMRM) has been designed, aiming at obtaining a structure lighter than modern commercially available equivalent reflectors, starting from available data of the mature mesh reflector family AstroMesh®. The dimensional stability of the payload is supposed to be constrained by using collocated smart piezoelectric actuators and sensors on the flexible structure. Their optimal location is studied by introducing a general and computationally efficient strategy to address the issue of actuators/sensors placement for generically-shaped 3-D flexible structures. In detail, both a gramian-based method and a solution exploiting the extraction of Modal Strain Energy from commercial finite element models and locations combinations computation are presented.

Then, the synthesis of a robust controller for performing the attitude control of the spacecraft, based on  $\mu$ -synthesis theory, is presented, being the plant of the system considered uncertain. Finally, the results from synthesis iterative process are discussed, along with the main results deriving from implementing both attitude and vibration control system on a plant considering also dynamic non-linearities. The control system proved to be able to reach the desired set-point angles by keeping the maximum displacement of the tip of the reflector under a sub-millimetre range, making such system suitable to high precision pointing operations.

As future developments, an unstructured synthesis combining both attitude and vibration control will be contemplated. Furthermore, more specific external disturbances (other than system non-linearities) as

orbital perturbations, solar pressure and thermal gradients could be considered in the study. In addition, failures and multiple piezoelectric anomaly behaviour will be considered to test the vibration control system efficacy.

## References

- [1] Ketner G.L., *Survey of historical incidents with Control-Structures Interaction and recommended technology improvements needed to put hardware in space*, Control Structures Interaction Office, NASA, Langley Research Center, Washington, 1989.
- [2] Belloch P. A., Beagley N. R., *Tools for analysis of control structure interaction*, Computer-Aided Engineering Journal, Vol. 7, Issue 4, August 1990
- [3] Xie Y., Huang H., Hu Y. et al., *Applications of advanced control methods in spacecrafts: progress, challenges, and future prospects*, Frontiers Inf Technol Electronic Eng 17, 841–861, 2016
- [4] Li Y., Sun Z., Ye D., *Robust linear PID controller for satellite attitude stabilisation and attitude tracking control*, International Journal of Space Science and Engineering 4(1):64, 2016
- [5] Benanni S., Ankersen F., Arcioni M. et al., *Robust Attitude Control Design for the BIOMASS Satellite (Earth Explorer Core Mission Candidate)*, Proceedings of the 18th IFAC Symposium on Automatic Control in Aerospace, 28 August – 2 September, 2011, Milan, Italy
- [6] Colagrossi A., Lavagna M., *Integrated vibration suppression attitude control for flexible spacecrafts with internal liquid sloshing*. Multibody Syst. Dyn., 2020.
- [7] Balas M. J., *Direct Velocity Feedback Control of Large Space Structures*, Journal of Guidance, Control, and Dynamics, Vol. 2, No. 3, pp. 252-253, 1979.
- [8] Fanson JL and Caughey TK, *Positive position feed- back control for large space structures*, AIAA Journal 28: 717–724, 1990.
- [9] Wie B., Ryson A.E., *Pole-zero modeling of flexible space structures*, J. Guid. Control Dyn. 11, 554–561, 1988.
- [10] Zhu L., Song W. and Hu Q., *Active vibration suppression and attitude maneuvers of flexible spacecraft via fuzzy sliding control*, 2008 Chinese Control and Decision Conference, Yantai, Shandong, pp. 3665-3669, 2008
- [11] Sabatini M., Palmerini G. B., Gasbarri P., *Synergetic approach in attitude control of very flexible satellites by means of thrusters and PZT devices*, Aerospace Science and Technology, Vol. 96, pages 2-11, January 2020



- [12] Astro Aerospace, *AstroMesh™ deployable reflector data sheet DS-409 07/04*, Northrop Grumman Space Technology, 2004
- [13] Morterolle S., Maurin B., Dubé J.F., Averseng J., Quirant J., *Modal behavior of a new large reflector conceptual design*, *Aerospace Science and Technology*, Elsevier, 42, pp.74-79, 2015
- [14] Santini P., Gasbarri P., *Dynamics of multibody systems in space environment; Lagrangian vs. Eulerian approach*, *Acta Astronautica*, Volume 54, Issue 1, Pages 1-24, January 2004;
- [15] Mazzini L., *The Dynamics of the Flexible Satellite. In: Flexible Spacecraft Dynamics, Control and Guidance*, Springer Aerospace Technology, Springer, 2016
- [16] Gasbarri P., Monti R., De Angelis C., Sabatini M., *Effects of uncertainties and flexible dynamic contributions on the control of a spacecraft full-coupled model*, *Acta Astronautica*, Vol. 94, Issue 1, pp. 515-526, Feb. 2014;
- [17] Angeletti F., Gasbarri P., Sabatini M., *Optimal design and robust analysis of a net of active devices for micro-vibration control of an on-orbit large space antenna*, *Acta Astronautica*, Vol. 164, pp. 241-253, Nov. 2019;
- [18] Angeletti F., Gasbarri P., Sabatini M., Iannelli P., *Design and performance assessment of a distributed vibration suppression system of a large flexible antenna during attitude manoeuvres*, *Acta Astronautica*, Vol. 176, pp. 542-557, Nov. 2020;
- [19] Ankersen F., *Guidance, Navigation, Control and Relative Dynamics for Spacecraft Proximity Maneuvers*, Doctoral thesis, Aalborg University, December 2015;
- [20] Alazar D., Cumer C., Tantawi K.H.M., *Linear Dynamic Modeling of Spacecraft with Various Flexible Appendages and On-board Angular Momentums*, 7th International ESA Conference on Guidance, Navigation & Control Systems (GNC 2008), 2 June 2008 - 5 June 2008 (Tralee, Ireland)
- [21] Piefort V., Preumont A., *Finite element modelling of piezoelectric active structures*, Doctoral Thesis, Université Libre de Bruxelles, Active Structures Laboratory Department of Mechanical Engineering and Robotics, 2001.
- [22] Gawronski W. K., *Advanced Structural Dynamics and Active Control of Structures*, Mechanical Engineering Series, Springer, New York, 2004;
- [23] Guo K., Jiang J., *Optimal Locations of Dampers/Actuators in Vibration Control of a Truss-Cored Sandwich Plate*, *Advances on Analysis and Control of Vibrations – Theory and Applications*, Sept. 2012
- [24] Doyle J., Packard A., and Zhou K., *Review of LFTs, LMIs, and  $\mu$* , *Proceedings of the 30th IEEE Conference on Decision and Control*, IEEE Publ., Piscataway, NJ, Dec. 1991, pp. 1227–1232.
- [25] Wang W. et al., *Verification and validation of attitude and orbit control system for flexible satellite*, *AIAA Guidance, Navigation, and Control Conference*, Chicago, 2009.
- [26] Skogestad S. and Postelwhite I., *Multivariable Feedback Control*, Wiley, Chichester, 1996
- [27] Doyle J.C., *Analysis of feedback system with structured uncertainties*, *Proc. IEE.D* 129, pp 242-250, 1982
- [28] Zhou, K., Doyle, J. C., *Essentials of robust control*, vol. 104, Upper Saddle River, NJ: Prentice hall, 1998

- The problem of designing an end to end architecture (from structural design to control laws verification) for attitude and vibration control for a large flexible antenna is addressed;
- A large antenna mesh reflector based on realistic space mission data is designed by using FEM techniques;
- A network of smart actuators/sensors including Piezo-stack actuators is developed;
- Different spatial configurations for the placement of actuators and sensors are investigated by using open-loops placement methods for generically shaped tri-dimensional structures;
- Attitude manoeuvres are performed to prove the efficacy of both the attitude and vibration control system.

Journal Pre-proof

**Declaration of interests**

The authors declare that they have no known competing financial interests or personal relationships that could have appeared to influence the work reported in this paper.

The authors declare the following financial interests/personal relationships which may be considered as potential competing interests:

Journal Pre-proof